

Effects of External Tidal Field on the Evolution of Multi-mass Star Clusters

K. H. Lee,^{1,2*} H. M. Lee³ and H. Sung¹

¹*Astrophysical Research Center for the Structure and Evolution of the Cosmos, Sejong University, Seoul 143-747, Korea*

²*Centre for Astrophysics & Planetary Science, School of Physical Sciences, University of Kent, Canterbury, Kent CT2 7NR, UK*

³*Astronomy Program, SEES, Seoul National University, Seoul 151-742, Korea*

12 September 2018

ABSTRACT

We present N-body simulations of realistic globular clusters containing initial mass function in the galaxy to study effects of tidal field systematically on the properties of outer parts of globular clusters. Using NBODY6 which takes into account the two-body relaxation correctly, we investigate general evolution of globular clusters in galactic tidal field. For simplicity, we have employed only spherical components (bulge and halo) of the galaxy. Total number of stars in our simulations was about 20,000. All simulations were done for several orbital periods in order to understand the development of the tidal tails. In our scaled down models, the relaxation time is sufficiently short to show the mass segregation effect, but we did not go far enough to see the core-collapse, and the fraction of stars lost from the cluster at the end of simulation is only about $\sim 10\%$. The radial distribution of extra-tidal stars can be described by a power law with a slope around -3 . The direction of tidal tails are determined by the orbits and locations of the clusters. We find that the length of tidal tails increases towards the apogalacticon and decreases towards the perigalacticon. This is an anti-correlation with the strength of the tidal field, caused by the fact that the time-scale for the stars to respond to the potential is similar to the orbital time-scale of the cluster. When the length of tidal tails decreases some of the stars in the tidal tails are recaptured by the host cluster. From the investigation of velocity anisotropy of the model clusters, we find that in the early stages of globular cluster evolution the clusters have radial anisotropy in the outermost parts, while clusters are nearly isotropic in the central region. The radial anisotropy decreases with time.

Key words: stellar dynamics - globular clusters: general - methods: *N*-body simulations

1 INTRODUCTION

Dynamical evolution of globular clusters is induced by a variety of internal and external processes. The main processes dominating the evolution of clusters are two-body relaxation and tidal shocks. Two-body relaxation makes the velocity distribution of stars towards Maxwellian and high-velocity stars gain enough energy to escape from the cluster (Spitzer & Thunan 1972). The external tidal shocks also accelerate the destruction of clusters (see, for example, Gnedin, Lee & Ostriker 1999). Clusters experience tidal shocks when they pass through the Galactic disk or close to the Galactic bulge. The escaped stars may remain in the vicinity of the cluster and form tidal tails for a while. Many observational studies show that the signs of the existence of tidal tails around

globular clusters (Grillmair et al. 1995; Grillmair et al. 1996; Holland, Fahlman & Richer 1997; Lehman & Scholz 1997; Leon, Bergond & Vallenari 1999; Leon, Meylan & Combes 2000; Testa et al. 2000; Odenkirchen et al. 2001, 2003; Sohn et al. 2003; Lee et al. 2003, 2004). The features of tidal tails are thought to be related to the orbit and location of the cluster and the Galactic potential. However the links between the properties of tidal tails and the cluster dynamics have not been fully understood yet. Combes et al. (1999) presented extensive N-body simulations of globular clusters, and showed the tidal effects quantitatively and geometrically. The main finding of Combes et al. (1999) is that there exist two giant tidal tails around the globular cluster along cluster's orbit. They also showed that the density distribution just outside the tidal boundary follows power laws to radius, and the extra-tidal stars form clumps which are the tracers of the strongest gravitational shocks. However,

* E-mail: khlee@arcsec.sejong.ac.kr

they used the PM method for the calculation of the gravitational potential: this method cannot take into account the two-body relaxation effect on the internal evolution of the clusters. Yim & Lee (2002) examined the general evolution of the globular clusters using NBODY6 which properly takes into account the effects of two-body relaxation. They showed that the density profiles of the clusters appear to become somewhat shallower just outside the tidal boundary as observed in many clusters and the directions of the tidal tails depend on the location in the galaxy as well as the cluster orbit.

Dynamical evolution of many body systems can be studied by various methods. The most desirable method to study dynamical evolution of a globular cluster is a direct N-body integration. However, this method becomes almost impossible to use as N becomes large, where N is the number of stars, since the computational time increases with N^3 . The required value of N (of order 10^6) is still beyond the capability of currently available computers. Fokker-Planck method has been commonly used as an alternative to direct N-body integration method. The main advantage of Fokker-Planck method is that it does not require much computing power. However, in this method, the shape of the cluster is restricted to sphere (or oblate spheroid for rotating models, see Einsel & Spurzem 1999) and the external gravitational field can be accounted for only approximately. To investigate tidal tails of globular clusters in the external potential realistically, we use N-body method in this study, but with significantly smaller number of N than realistic globular clusters. We will focus on the behavior of stars especially in the outer parts of the globular clusters. This paper is organized as follows. In Sect. 2, we briefly describe the method and models. And the results of simulations are described in Sect. 3. The final section summarizes our major findings.

2 METHOD AND MODEL

2.1 NBODY6++

N-body simulations for this study have been carried out using NBODY6++ which is a parallelized version of NBODY6 developed by Aarseth to use parallel super computer (Spurzem 1999). We modified the program to include external potential, which is described in §2.2. The code uses a direct summation method in computing the gravitational potential and adopts Hermite integration scheme which is simple to use and highly effective for advancing the single particles. The main idea of Hermite integration scheme is to employ a fourth-order force polynomial but now the two first terms are evaluated by explicit summation over all N particles, thereby enabling two corrector terms to be formed. The code also adopts an Ahmad-Cohen neighbor scheme (Ahmad & Cohen 1973) which is based on the idea of separating the total force on a particle into two components,

$$F = F_{irr} + F_{reg}.$$

where F_{irr} is the irregular force caused by relatively nearby stars and F_{reg} is the regular force from rather distant stars. The irregular force varies with time rather rapidly while the regular force changes slowly. Since the external force due to the host galaxy is expected to vary rather slowly, we regarded such force as a regular one. Each part is represented

by the high-order force polynomial on its own time-step. The neighbor force is updated on a time-scale determined by the local fluctuations, whereas the smoother regular component due to all other members need only be recalculated on a longer time-scale, with intermediate values obtained by prediction. At each regular time-step a new neighbor list is determined using a given neighbor radius for each particle. It also includes the formation of binaries via three-body processes and their interactions with other stars. The main force loop in NBODY6 is decomposed in three independent DO-loops, advancing all the regularized binaries (1), computing new irregular forces and applying the corrector due to them (2), and computing new regular forces, new neighbor lists and applying the regular force corrections (3). The entire content of the routines relevant to (2) and (3) have been parallelized in NBODY6++. This is all done fully in parallel for the different particles due in this block (Spurzem & Baumgardt 2002). Detailed mechanisms of NBODY6 are described in Aarseth (1999, 2004) and references therein.

2.2 The Model Galaxy

The gravitational potential of the Galaxy is generated by stars, gas, and dark matter. There is no single numerical method that can describe the evolution of the Galaxy since there are many components that react differently. Further, we expect that the time-scale for the variation of Galactic potential would be much longer than the orbital time-scale of the clusters. Therefore the Galactic potential is assumed to be independent of time for simplicity. The main components of the Galaxy are central bulge, disk, halo, and bar. In the present study, the model Galaxy is assumed to be composed of two components: halo and bulge, to focus on the effects from spherical components only. We have used simple model potentials following Lee et al. (1999). The halo component, which gives rise to the flat rotation curve at large radii, is assumed to have a logarithmic potential,

$$\Phi(r)_{halo} = \frac{1}{2}v_0^2 \ln(R_c^2 + r^2) + const,$$

where R_c is the halo core radius and v_0 is the constant rotation velocity at large r . As for the bulge component, we have assumed the Plummer model to allow a steep outward velocity increase from the Galactic centre (Binney & Tremaine 1987),

$$\Phi(r)_{bulge} = -\frac{GM_{bulge}}{\sqrt{r^2 + r_c^2}},$$

where r_c is a parameter that controls the size of bulge. The bulges of real galaxies can be better represented by de Vaucouleurs's $R^{1/4}$ law, but we have chosen the Plummer model for simplicity. Our model have $r_c \simeq 230 \sim 240$ pc. In our numerical calculations all physical quantities are given with dimensionless units. The unit of length is chosen to be $R_{sc} = 10$ kpc. The total mass of the Galaxy within 10 kpc is assumed to be $M_{10} = 1.24 \times 10^{11} M_\odot$ (Caldwell & Ostriker 1981). The unit of velocity is $v_{sc} = (GM_{10}/R)^{1/2} \simeq 230.7$ km/s. In these units, the rotation velocity v_0 at the distance of 10 kpc is 0.92 and $M_{bulge} = 0.08$, $R_c = 0.7$.

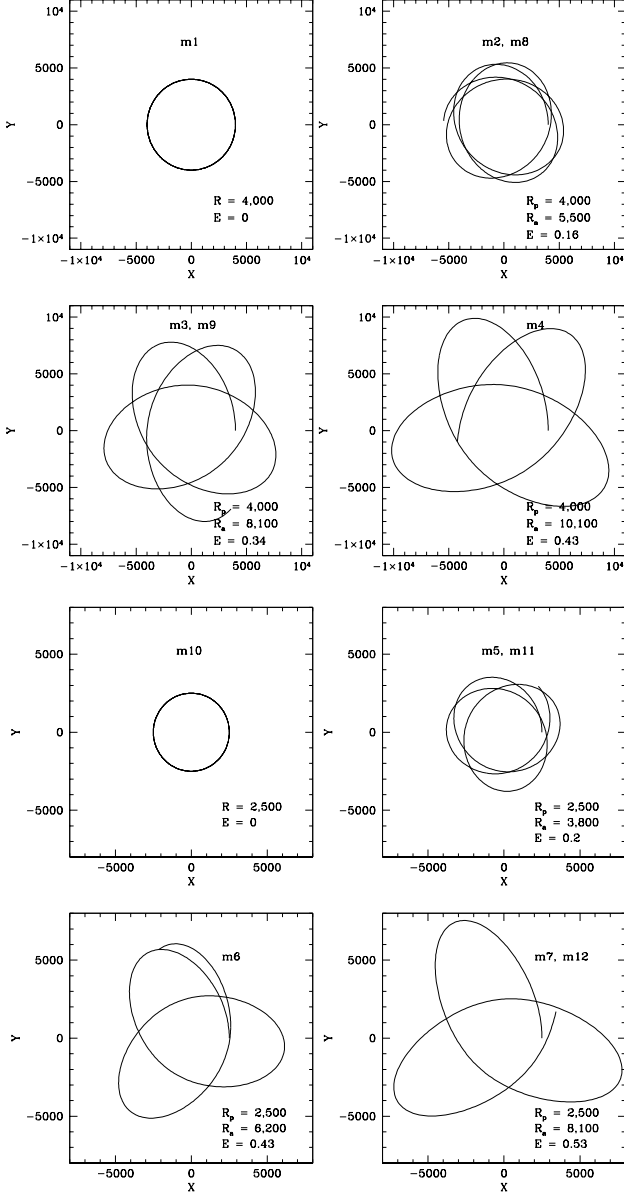


Figure 1. Orbits of model clusters. R_p is distance of the perigalacticon, R_a is distance of the apogalacticon, and E is the ellipticity of orbits.

2.3 Initial Conditions of Globular Clusters and Their Orbits

We have used the King model with $W_0 = 5$ and $W_0 = 7$ as initial models, where W_0 is the scaled central potential, which determines the degree of central concentration (King 1966). The density profiles of all mass components are assumed to be the same at the beginning (i.e. no initial mass segregation). We choose the initial mass spectrum to be a simple power law

$$dN(m) \propto m^{-\alpha} dm,$$

where $dN(m)$ is the number of stars with masses between m and $m + dm$, and we have chosen $\alpha = 2.35$ which represents a Salpeter initial mass function. The range of mass in our models is from 1 to 10 M_\odot . The total mass of a cluster is

Table 1. Parameters of the cluster models and orbits.

Model	W_0	r_c (pc)	r_t (pc)	r_{peri} (kpc)	r_{apo} (kpc)	E	Period (Myr)
m1	5	2.5	25	4	4	0	167
m2	5	2.5	25	4	5.5	0.16	242
m3	5	2.5	25	4	8.1	0.34	294
m4	5	2.5	25	4	10.1	0.43	331
m5	5	1.5	16	2.5	3.8	0.20	191
m6	5	1.5	16	2.5	6.2	0.43	238
m7	5	1.5	16	2.5	8.1	0.53	270
m8	7	0.8	25	4	5.5	0.16	242
m9	7	0.8	25	4	8.1	0.34	294
m10	7	0.6	16	2.5	2.5	0	105
m11	7	0.6	16	2.5	3.8	0.20	191
m12	7	0.6	16	2.5	8.1	0.53	270

$M = 4.2 \times 10^4 M_\odot$, and the number of stars is $N = 18,809$. We have ignored the effects of stellar evolution in order to concentrate on the pure dynamical processes and also for simplicity. We have carried out a total of 12 simulations with different cluster orbits. For models with elongated orbits, we defined the ellipticity as,

$$E = \frac{R_a - R_p}{R_a + R_p}$$

where R_a and R_p are apogalacticon and perigalacticon, respectively. The parameters of models are listed in Table 1, and the cluster orbits are shown in Fig. 1. We have removed the stars from our simulations when the distance from the cluster centre exceeds five times of the tidal radius. The tidal radius r_t of the cluster is defined as,

$$r_t \equiv \left(\frac{M_c}{2M_G} \right)^{1/3} R_a,$$

where M_c is the cluster mass, and M_G is the galactic mass within radius R_a . Here we have assumed that the tidal radius is determined by the tidal force at the apogalacticon. We are mostly interested in the development of tidal tails, and thus we do not follow the cluster until its destruction.

2.4 Time-Scale Consideration

The number of stars of around $N \sim 20,000$ used in the present study is clearly much smaller than that of realistic globular clusters. Different dynamical processes operate on different time-scales. The cluster's orbit depends only on the orbital parameters (such as the ellipticity and peri- or apo-galacticon distance), and not on N . The orbital time of the stars near the tidal boundary is also very close to the orbital period of the cluster. However, the dynamical evolution such as core-collapse and mass segregation take place in two-body relaxation time-scale. Since the relaxation time depends on local variables such as stellar density and velocity dispersion, a single representative value was defined as ‘half-mass relaxation time’ by Spitzer & Hart (1975) as

$$t_{rh} \equiv 0.138 \frac{N^{1/2} r_h^{3/2}}{m^{1/2} G^{1/2} \ln(0.4N)},$$

where r_h is the radius within which the enclosed mass is the half of the total mass and m is the mass of the individual stars. For clusters with mass function, m is not a well defined

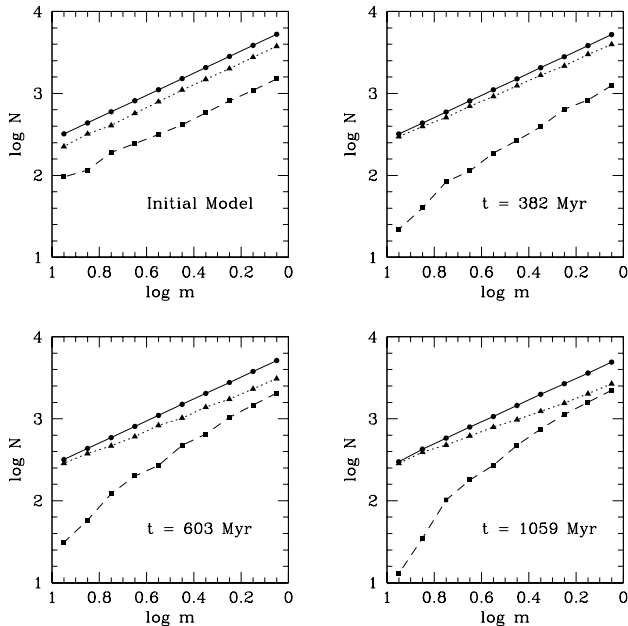


Figure 2. Mass functions of model m3 at a few selected epochs. Filled circles, MF from the whole stars; filled triangles, inner region; filled squares, outer region. We can see that mass segregation effect increases with time.

parameter, but we can simply replace it by the mean mass although there is no clear reason (see Lee & Goodman 1995 for more discussion). As we can see from the above equation, $t_{rh} \propto N^{1/2}$. This means that the dynamical evolution of our models takes place much faster than real globular clusters for a given orbital period. The initial half-mass relaxation time of our model is about 3.7×10^8 yr which is much shorter than those of real globular clusters. The evaporation time-scale is also proportional to the half-mass relaxation time (Henon 1961, Lee & Ostriker 1986), and thus we expect the development of the tidal tails would be also relatively fast. However, since our simulation would last for only up to about 10^9 years, the entire evolution we observe from the simulation could be comparable to that of real globular clusters.

The amount of time for stars remaining in the tidal tails is expected to be of order of orbital time-scale of the cluster (e.g., Lee & Ostriker 1986), which is not related to the number of stars. Therefore, the dynamical features in the tidal tails of our simulation would not be affected by the fact that we used the smaller number of stars than realistic clusters. In Table 1, we have listed the radial period which is the time from perigalacticon to next perigalacticon of orbits in units of years for our models.

3 RESULTS

3.1 Mass Segregation

During the dynamical evolution of the globular cluster, the stars in the cluster try to achieve energy equipartition, so that all stars have the same kinetic energy. It causes the process that higher mass stars slow down and sink towards the central region of the cluster, whereas the lower mass stars

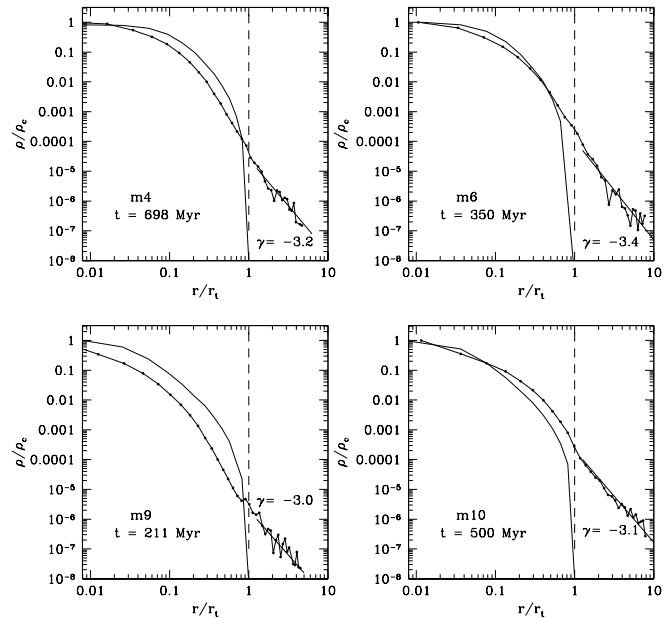


Figure 3. Radial density profile of models m4, m6, m9, and m10. The initial profiles are shown for comparison. Note the clear indication of tidal tails. The average power law gradient is -3.2 .

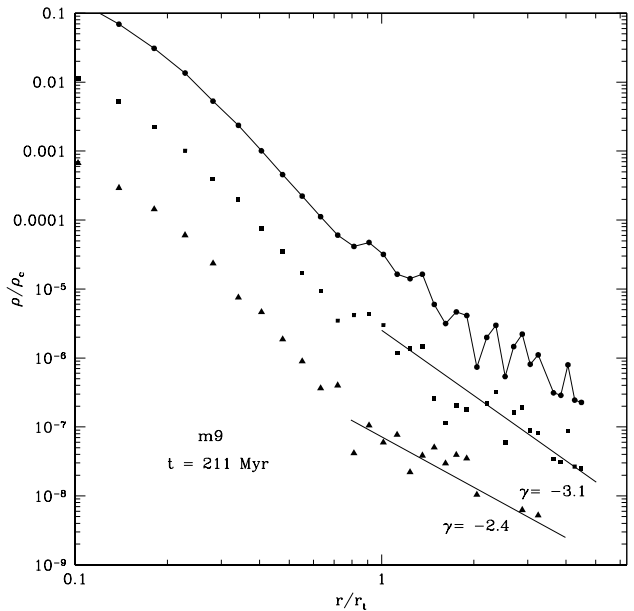


Figure 4. Fit of power laws to the external profile of model m9. Triangle, the profile of massive stars; filled squares, the profile of less massive stars; filled circles, the profile of all stars; solid lines are the fitting power laws. The profile of less massive stars shows a steeper slope.

have higher velocities than the mean and tend to occupy the outer region of the cluster. This process is called mass segregation (Spitzer 1987). Many observational studies have shown the mass segregation effect in many globular clusters. As a result of mass segregation, the envelope of a cluster is preferentially populated by low-mass stars, so they escape from the cluster more easily than the high-mass ones. Unlike

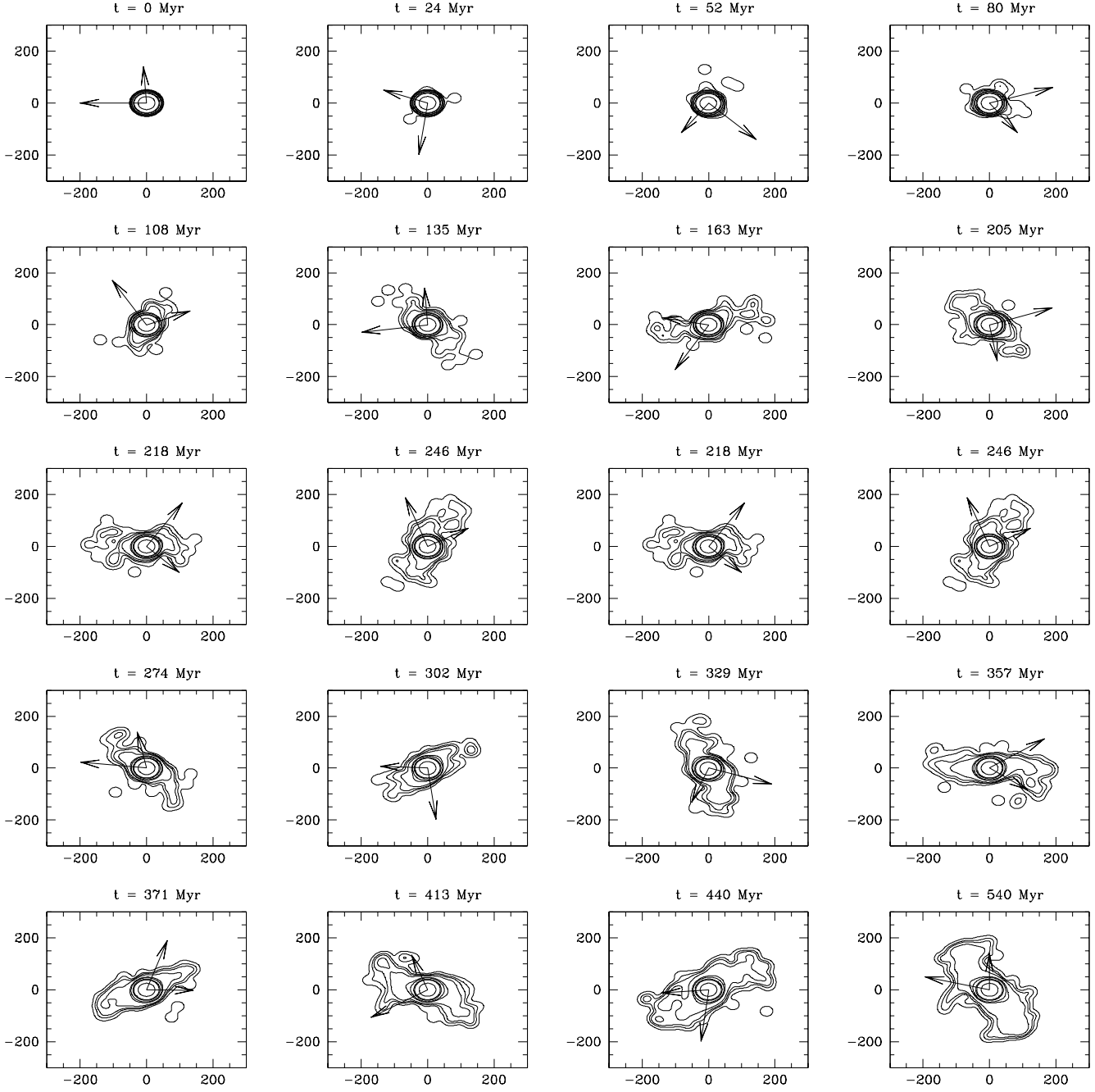


Figure 5. Development of tidal tails of model m5. Each time step is marked as Myr. Two arrows of each panel indicate the directions of the galactic centre (long) and its orbit (short). The unit of coordinate is pc.

our work, Combes et al. (1999) have employed models with low mass stars being more populated in the outer parts to mimic the clusters that have reached the mass segregation, since their models do not include the two-body relaxation effects. In the present study, we used models which have no initial mass segregation but evolve towards the segregated state automatically. We can see the process of mass segregation in the variation of mass functions (MFs) of globular clusters with time. The MF can be represented by a power law shown in the previous section. The slope of mass func-

tions becomes steeper in the outer part of the cluster as a result of mass segregation.

Fig. 2 shows the MFs of model m3 at a few selected epochs. In the initial models, MFs are the same in all regions, but the evolved models clearly show that the MFs depend on the position in the cluster. We can see that the massive stars are more concentrated to the inner region while the less massive stars are dominant in the outer region. As a result, the MFs of outer region are steeper than those of inner region. We can also see that the mass segregation effect increases with time. Because of preferential migration of

high-mass stars towards the centre, the slope of MF from the inner region tends to be more flattened with time. However the slope of MF from the whole region does not change very much until $M \sim 0.5M_i$, where M_i is initial mass of a cluster (Lee, Fahlman & Richer 1991; Takahashi & Lee 2000). Since the main purpose of our simulation is to examine the development and evolution of tidal tails, we did not continue the simulations towards the significant loss the total mass. Thus the MF of the entire cluster does not change significantly until the end of our simulations, but the outer parts of the clusters become quickly dominated by low mass stars since the mass segregation takes place much faster than the evaporation time-scale.

3.2 Radial Density Profile

Indications of tidal tails around globular clusters have been found in several previous studies of globular cluster radial density profiles. For a given tidal field, the outer part of a globular cluster has more stars than that of a King model. As a result, the slope of the radial density profile shows a deviation from the King model around the tidal radius of the cluster. We show some of the examples in Fig. 3. The initial profiles are shown for comparison.

The radial distribution of extra-tidal stars can be described by a power law $\Sigma(r) \propto r^{-\gamma}$. We derived the average value of $\gamma = -3.2$ from the simulations. This value is in well accordance with Combes et al. (1999) who deduced a slope around $\gamma = -3$ from their N-body simulations. The reason for such a steep slope is that the stars in the tidal tails are preferentially on radial orbits, and the gravitational potential is almost Keplerian. It has long been known that the density profile falls like $r^{-3.5}$ in such a case.

On the other hand, the observed globular clusters tend to have shallower slopes. The observed studies of Grillmair et al. (1995) and Leon et al. (2000) showed that most of the slopes are around -1 . Lee et al. (2003) found that the slope of Galactic globular cluster M92 is $\gamma = -1.27$ from the deep CCD photometry. Combes et al. (1999) explained the shallower slope in the observations as the contamination of background-foreground populations. Although this must be a main source of discrepancy, we could consider other reasons. As an example, Lee et al. (2003) showed that the slopes of the density profiles for stars in different magnitude bins have different values in the outer part.

Testa et al. (2000) obtained the surface density profile of M92 using plates from the Digitized Second Palomar Sky Survey. They fitted the extra-tidal profile of the cluster to a power law and found $\gamma = -0.85 \pm 0.08$. Lee et al. (2003) derived $\gamma = -0.82 \pm 0.10$ using only the bright stars ($18.5 < V < 20.5$), which correspond with the stars in the study by Testa et al. (2000) from surface density profile of M92. Whereas, using the faint stars ($22 < V < 23.5$), they found a steeper slope of $\gamma = -1.31 \pm 0.09$, which is significantly different from that of the bright stars.

We found similar trends in our results of N-body simulations. In Fig. 4, we show an example radial density profiles for different masses in model m9. We can see that the profile of massive stars have shallower slope than that of less massive stars. The profile of massive stars ($2M_\odot < M < 10M_\odot$) follows a slope of $\gamma = -2.4$ while that of less massive stars ($1M_\odot < M < 2M_\odot$) have a much steeper slope of $\gamma = -3.1$.

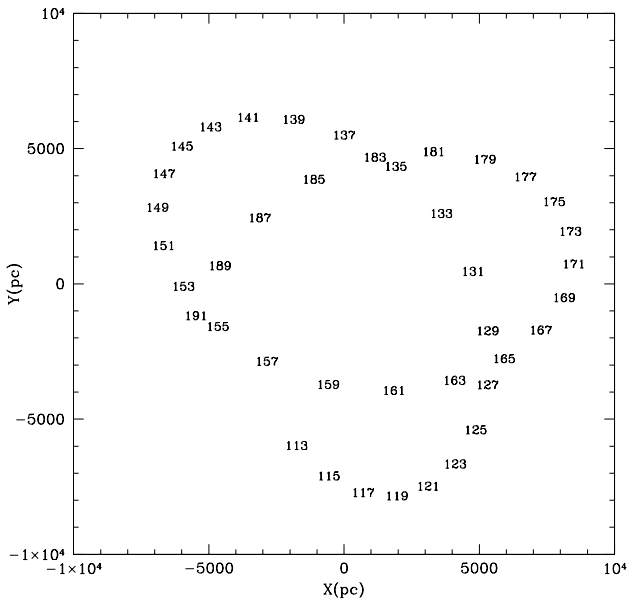


Figure 6. The orbit and location of each step of model m3. Step numbers are marked.

This implies that the difference in slopes of the density profiles in different magnitude bins is a real feature of the clusters. Most of observational studies have used only bright stars, because of the sensitivity of the photometry. This could be a part of the reason for the shallower density distribution in observational data. The velocity anisotropy depends on the mass of the stars, and the higher mass stars tends to be on more tangential orbits than lower mass stars (see, for example, Takahashi & Lee 2000). The stars with less radial anisotropy would be populated in shallower profile.

Since the tidal tails of globular clusters are preferentially formed by the lowest mass stars (Combes et al. 1999), it is difficult to study tidal tails of globular clusters using only bright stars. This means that the study of globular clusters tidal tail should be performed using stars with the lowest possible mass that is detectable. Deep CCD studies of other nearby clusters are needed to verify whether the mass dependence of the density profile slope is a common phenomenon.

3.3 Tidal Tails

The stars unbound from the host cluster do not escape instantaneously, but they slowly drift from the globular cluster and form tidal tails. They can form well-defined features outside the cluster, as observed on the sky (Lee et al. 2003 and references therein). The development of tidal tails of one model (m5) is displayed in Fig. 5. Two arrows indicate the direction of galactic centre (long) and cluster orbital direction (short). The maps are projected in the (X,Y) plane on which the cluster orbits. We can see the development of almost symmetrical tidal tails in two directions.

The directions of tidal tails are known as a good tracer of cluster orbital phase. Combes et al. (1999) presented from N-body simulations that there exist two tidal tails around the globular cluster along its orbit. In large scale, it seems obvious that the tidal tails would be aligned with the clus-

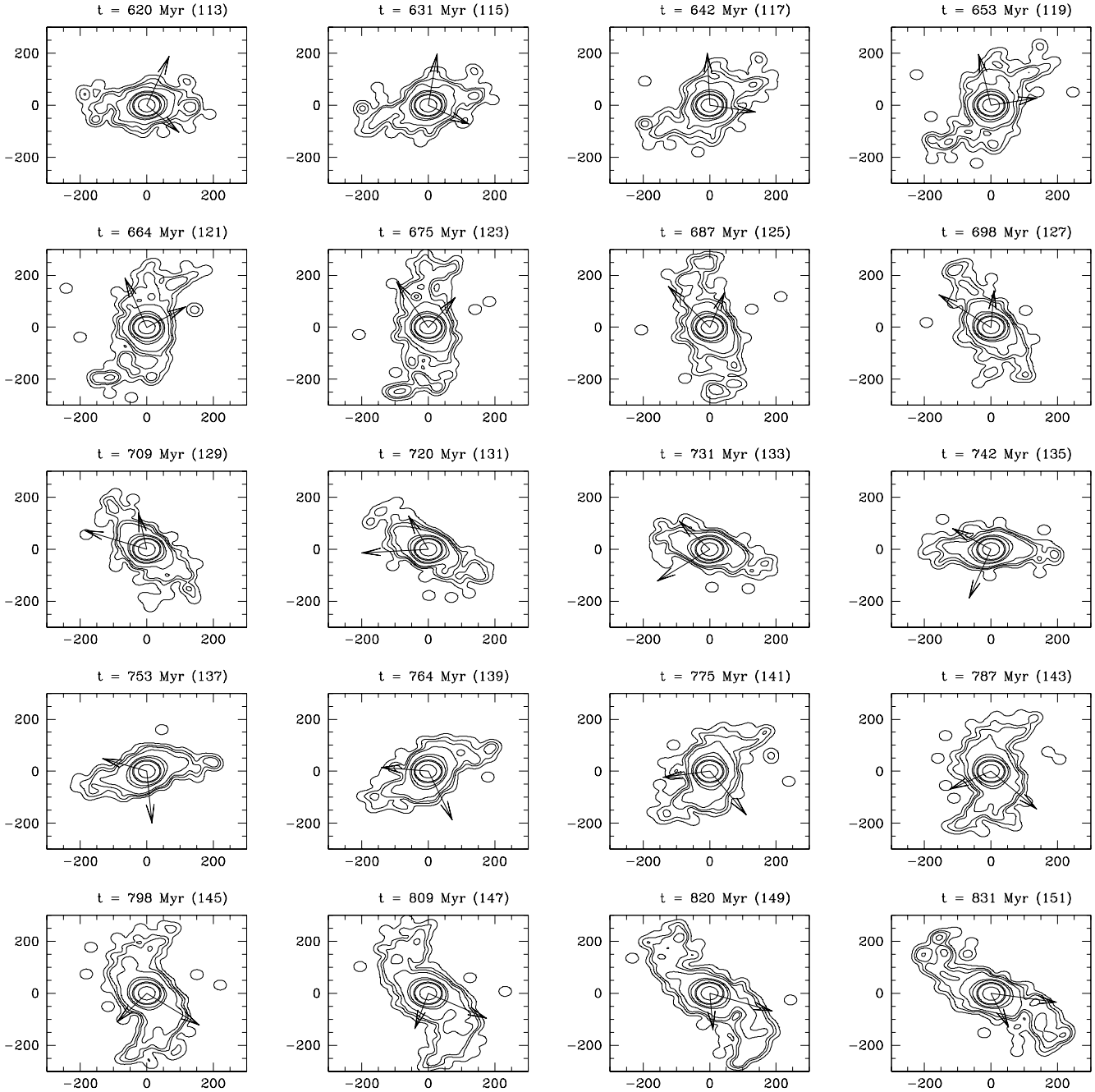
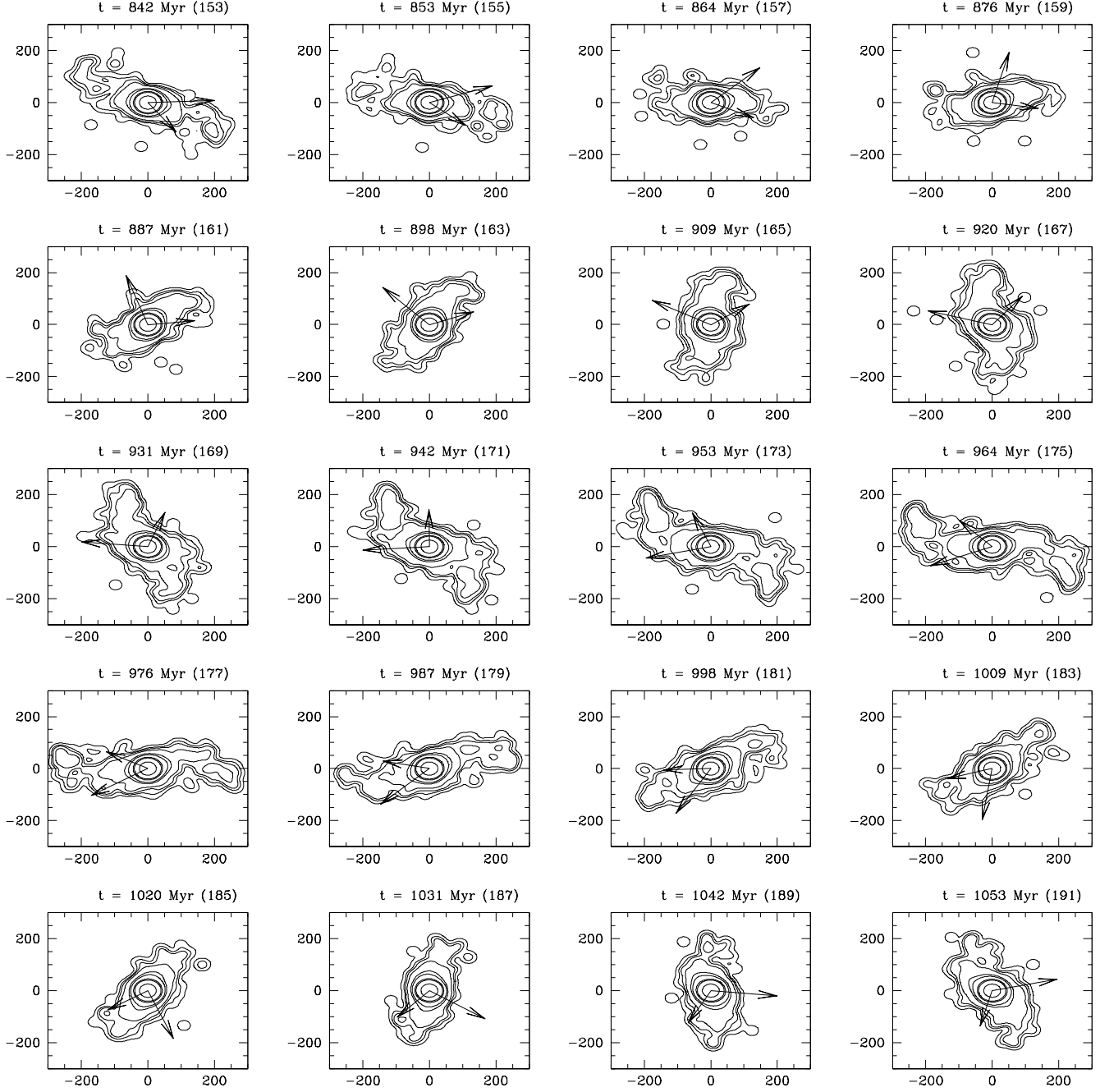


Figure 7. Contours of levels of model m3. Each time-step is marked as Myr and step number. The positions of each time step in the orbit can be traced by step numbers in Fig. 6. Two arrows of each panel indicate the direction of the galactic centre (long) and its orbit (short). Note the change of length of tidal tails. The unit of coordinate is pc.

ter's orbit. Recently, Odenkirchen et al. (2001, 2003) detected clear tidal tails around the Galactic globular cluster Palomar 5, extending over an arc of 10° on the sky, corresponding to a projected length of 4 kpc at the distance of the cluster. They also showed that the tidal streams are aligned with the orbit of this cluster. However, not all globular clusters show such clear tidal tails like Palomar 5. Actually, Palomar 5 is the first, and only globular cluster whose tidal tails have been detected at a very significant level of confidence so far. Most of observational studies about globu-

lar clusters do not cover such a large scale either. In present study, we focused on a variation of tidal tails of globular clusters along its orbits in a relatively small scale (within $5r_t$). We found that in small scale, the directions of tidal tails of globular clusters are not consistent with its orbital direction. In Fig. 6 and Fig. 7, we show the positions in the orbit of one model (m3) and its contours of levels. To see the direction of tidal tails, we show the θ/θ_0 as a function of time for model m3 in Fig. 8. Here, θ_0 is the angle between the directions of galactic centre and orbital motion, and θ is

Figure 7 – *continued*

the angle between the directions of galactic centre and tidal tail. We can see that the direction of tidal tails is almost median of the directions of galactic centre and cluster orbit in all galactic positions.

From these figures, we also find the relation between the length of the tidal tails and the orbital phase of the cluster. The cluster which has a circular orbit shows almost the same length of tidal tails since the strength of tidal tails does not change with time. However in the elliptical orbit, the lengths of tidal tails change with time depending on the galactocentric distances R_G . The clusters on elongated orbits experience variation in tidal field. If the Galactic potential

behaves like Keplerian, the tidal force is proportional to R_G^{-3} while the logarithmic potential gives rise to the R_G^{-2} dependence. In any case, the amount of the variation in tidal force for clusters on elongated orbits would be significant. We may simply assume that the tidal tails would be longer when the tidal force is stronger.

However, from Fig. 6 and Fig. 7, we can see that the length of the tidal tails increases towards the apocentre where the tidal force from the bulge is weakest (near orbit number 147 and 173 in Fig. 6) and decreases towards the pericentre. Yim & Lee (2002) first noted such behavior, and explained that the stars usually do not respond instan-

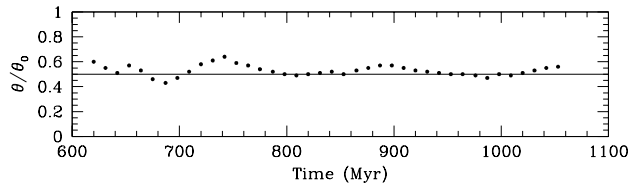


Figure 8. Direction of tidal tails of model m3. θ_0 is the angle between the directions of galactic centre and orbital motion, and θ is the angle between the directions of galactic centre and tidal tail. The direction of tidal tail is almost median of the direction of galactic centre and cluster orbital direction.

taneously to the external force. Since the stars near the tidal boundary have orbital periods similar to the cluster's orbital time around the galaxy, the effect of the strongest tidal force appears when the tidal force is weakest.

3.4 Extra-Tidal Stars

The stars in the tidal tails can be called as extra-tidal stars. We show the fraction of these stars as a function of time for all runs in Fig. 9 and Fig. 10. The definition of extra-tidal stars is clear only when the globular cluster is embedded in a steady potential, which is the case for a circular orbit. A common approximation is to assume that a star is unbound when it exceeds the conventional tidal radius (Meylan & Heggie 1997), and N-body models show that this leads to consistent results (Giersz & Heggie 1997). However, for the elongated orbits, the tidal radius varies along the orbit. Keenan (1981) found that the limiting radii of observed globular clusters are close to the tidal radius at pericentre. In this study, simply the stars which lie outside the tidal radius are regarded as extra-tidal stars. For the elongated orbits, the tidal radius at pericentre have been used as limiting radius. In calculation of the fraction, the stars eliminated from the simulations which went beyond the 5 times of tidal radius were also included in extra-tidal stars.

Generally the fraction increases with time, but the clusters having elongated orbits show clear decrease at some points (in models m3, m4, m6, m7, m9 and m12). In Fig. 10, we show the variation of the fraction of extra-tidal stars of model m9 which has eccentricity of 0.34. The arrows in Fig. 10 denote the pericentre in the orbit of m9. We can see that the fraction of extra-tidal stars reaches small peaks at the pericentre and then slightly decreases. These points correspond to the time when the length of tidal tails decreases. We can see that when the length of tidal tails decreases part of the stars included in tidal tails are recaptured by the host cluster.

In addition, from the comparison of m2 and m5 in Fig. 9, we can see the effect of strengths of external potential on the rate of evaporation of stars. With the same initial cluster model, the one which has closer orbit from the galactic centre (m5) shows steeper increase in the fraction of extra-tidal stars. Obviously, the clusters in stronger tidal fields experience more rapid evaporation of stars.

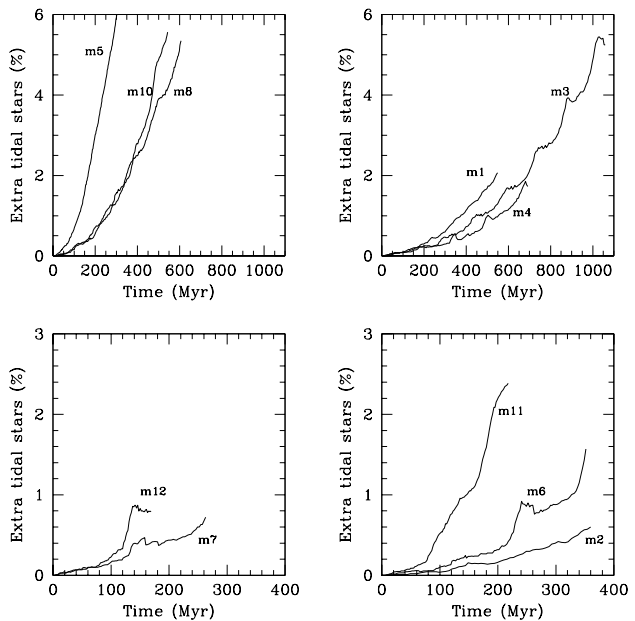


Figure 9. Fraction of extra-tidal stars as a function of time for all runs except m9. Note that the models having elliptical orbits show clear decrease at some points.

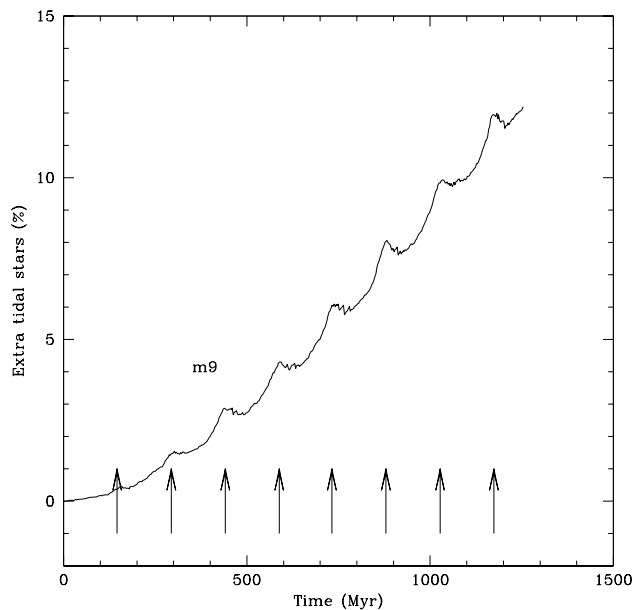


Figure 10. Fraction of extra-tidal stars as a function of time for model m9. The arrows denote the pericentre in the orbit. The fraction makes small peaks at the pericentre and then slightly decreases.

3.5 Angular Momentum

The model clusters used in this study have no angular momentum at the beginning. However, the probability that the globular clusters is formed without initial angular momentum is very small. A seed angular momentum in a proto-cloud would remain in the globular cluster without dissipation, since the time-scale of cluster formation is much shorter compared to globular relaxation times. White &

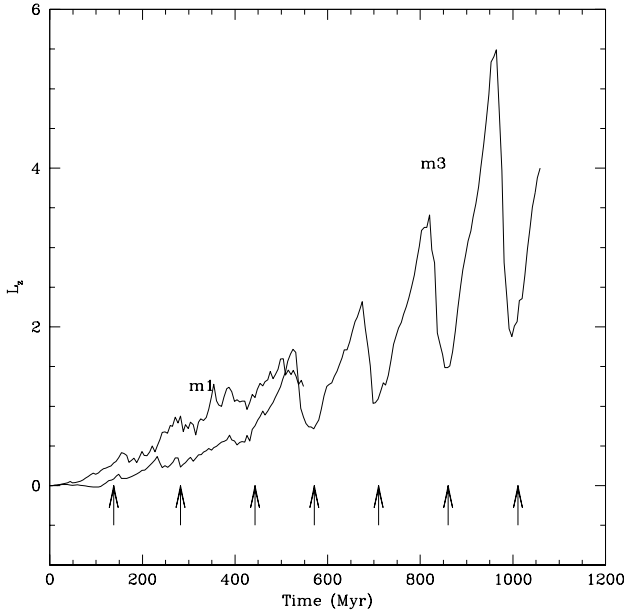


Figure 11. Z component of specific angular momentum of clusters as a function of time for models m1 and m3. The arrows denote the pericentre of model m3 having elliptical orbit.

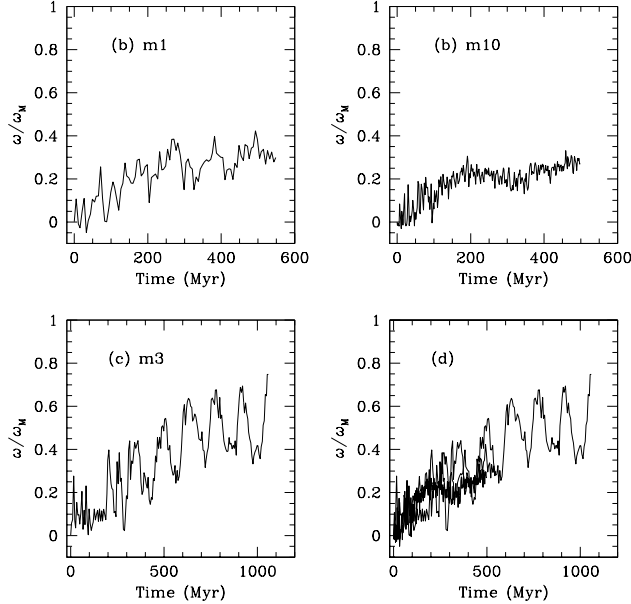


Figure 12. The angular speed of model clusters. The values are normalized by the maximum angular speed (orbital angular speed) of each orbit. 3 models are plotted altogether in panel (d).

Shaw (1987) have measured the projected axial ratio (b/a) of 100 globular clusters in the Milky Way, where a and b denote semi-major and semi-minor radii, respectively. They obtained that mean axial ratio $\langle b/a \rangle = 0.93 \pm 0.01$. They argued that the flattened shape of the clusters can be caused by either anisotropy in velocity dispersion or rotation. Since the velocity distribution of stars in tidally truncated clusters tends to become quickly isotropic (Takahashi & Lee 2000), the flattening is likely to be caused by rotation (Combes

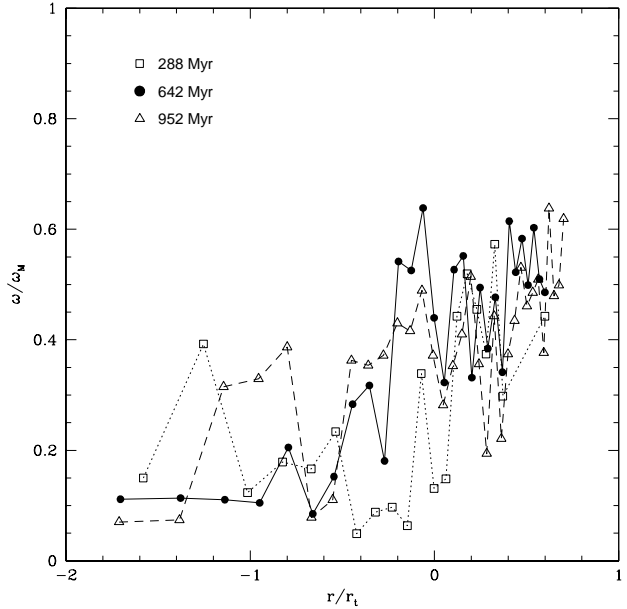


Figure 13. The angular speed of model cluster m3 along the equator at a few selected epochs. The values are normalized by the maximum angular speed (orbital angular speed).

1999). Kinematical data also showed that the flattening could be explained by rotation, and that the minor axes are nearly coincident with the rotation axes (Meylan & Mayor 1986).

Einsel & Spurzem (1999) demonstrated that the influence of rotation on star cluster evolution is not small. The core-collapse time could be accelerated significantly by initial rotation. Though rotation is a natural initial condition from collapse of a star-forming cloud, it is not easy to include the rotation in most of the existing evolutionary models of star clusters. Kim et al. (2002) showed that the evolution of the tidally limited cluster is significantly accelerated by initial rotation for equal mass models. Recently, from the multi-mass Fokker-Planck models, Kim, Lee & Spurzem (2004) confirmed that the rotation accelerates core-collapse and dissolution of globular clusters even for multi-mass models.

The initial angular momentum is expected to disappear from the cluster with time by the escape of stars carrying some angular momentum. Frenk & Fall (1982) showed that the young globular clusters are flatter on average than old ones in the LMC. Globular clusters with shorter relaxation time are also rounder (Davoust & Prugnel 1990), which supports the loss of rotation with relaxation. Kim et al. (2002, 2004) showed that the rotational energy in unit of total energy decreases monotonically with time in the tidally limited rotating clusters. However, the clusters could acquire angular momentum through tidal interactions with the Galaxy. We show the Z component of specific angular momentum (angular momentum per unit mass) of clusters as a function of time for models m1 and m3 in Fig. 11. The arrows in Fig. 11 denote the pericentre of model m3 having elliptical orbit. The two models have the same initial conditions except for their orbits. Fig. 11 shows that the clusters gradually acquire angular momentum by tidal torque. The model m1

having circular orbit (maintaining closer distance from the Galactic centre) has steeper increase in angular momentum. In model m3 having elliptical orbit, just after the perigalactic passages, the cluster angular momentum shows rapid increase. From these results, we can conclude that the Galactic tidal field play an important role in providing angular momentum to the clusters. The peaks of angular momentum appear near apocentre where the length of tidal tails is maximum.

The maximum angular speed acquired by tidal torque would be the synchronous speed, which means the cluster rotates at the same angular speed as the orbital angular speed. We show the angular speed normalized by maximum angular speed (orbital angular speed) at the tidal radius of clusters as a function of time for three models in Fig. 12. We can see that the angular speed increases with time, but our simulations do not last long enough to achieve the synchronous rotation. When the results for three different orbits are folded together as shown in Fig. 12(d), the behavior of angular speed evolution appears nearly the same for all. We can not find any clear difference between orbits (Fig. 12(d)) possibly because of short time coverage. In case of the model m3 (covering the longest time), the angular speed would reach the maximum in about 7 times orbital period if it linearly increases.

If a fully relaxed globular cluster has a significant rotation it would be the result of tidal interactions with the Galaxy because the initial rotation decrease with time and finally disappear (Kim et al. 2002, 2004). Lee et al. (2004) suggested that the globular cluster NGC 7492 which has significantly flattened shape has been much affected by tidal shocks from the relatively flat MF slope and its small mass. If the flattened shape of NGC 7492 is caused by its rotation, Galactic tidal field must have given important influences. When we get the radial velocity distribution, we will be able to verify the role of tidal field in rotating of this cluster.

From the radial profiles of the rotational velocity Kim et al. (2002, 2004) showed that the rotational velocities of initially rotating clusters decreases beyond the half-mass radius. As an observational result, the rotation of the bright Galactic globular cluster ω Centauri is almost solid-body until about 15% of the tidal radius, and then falls off quickly (Meylan & Mayor 1986, Merritt, Meylan & Mayor 1997). However, we found that the rotating clusters accelerated by tidal torque have different shape of radial angular speed distribution from initially rotating clusters. In Fig. 13, we have shown the distribution of angular speed as a function of radius for model m3. Although the data are rather noisy, the angular speed starts from a differential rotation with higher angular speed at larger radii to rigid body rotation. This is due to the fact that the tidal torque is more effective at the outer parts, but the inner parts gets the angular speed through the relaxation. The rotational energy for a uniformly rotating stellar system with angular speed ω is around $Mr_t\omega^2$ and maximum value of ω obtained by the tidal torque is $\sim v_{rot}/R_G$, where v_{rot} is the velocity of galactic rotation. The ratio of rotational kinetic energy to gravitational potential energy can thus become $T_{rot}/W \sim \left(\frac{r_t}{R_G}\right)^2 \left(\frac{v_{rot}}{\sigma}\right)^2$, where σ is the velocity dispersion of the cluster. For a cluster at $R_G = 5$ kpc, $r_t = 25$ pc, and $\sigma = 5$ km/s, T_{rot}/W could be about 0.05. Such an amount

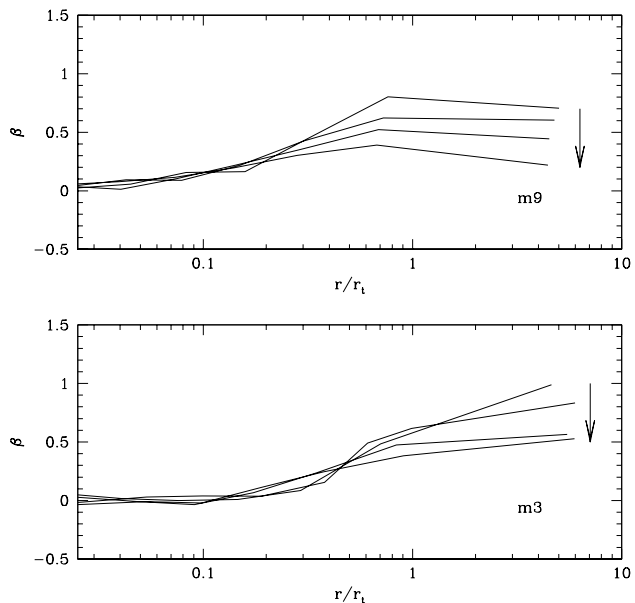


Figure 14. The radial variation of anisotropy parameter of models m1 and m3. m1 has time range of 132 \sim 554 Myr, and m3 has 133 \sim 1065 Myr. All models show radial anisotropy in the outer parts of the clusters and the radial anisotropy decreases with time.

of rotation could produce the dynamical ellipticity greater than 0.1 (e.g., Kim et al. 2002).

3.6 Velocity Anisotropy

It has long been known that isolated star clusters become radially anisotropic after core-collapse due to the scattering of stars out of the cluster core (Spitzer 1987). The development of velocity anisotropy was investigated in some works which used various numerical methods. Most of these calculations confirmed the earlier expectations of generation of radial anisotropy in the outer parts of the clusters, although the detailed behavior depends on the numerical methods. However, actual clusters are embedded in the Galactic tidal field which should impose a finite boundary to the cluster. The introduction of tidal boundaries gives significant effects on the velocity anisotropy because the stars could outflow over tidal boundary. Giersz & Heggie (1997) found in N-body simulations that star clusters in tidal fields remain isotropic during their evolution except for the outer parts which become tangentially anisotropic due to the preferential loss of stars on radial orbits. Takahashi & Lee (2000) found in their anisotropic Fokker-Planck simulations that the clusters develop stronger radial anisotropy in the outer part of the cluster during the early phase and then the development of radial anisotropy stops, and finally strong tangential anisotropy appears as the cluster loses mass. Recently, Baumgardt & Makino (2003) showed with N-body simulations that the outer parts of the clusters become rapidly tangentially anisotropic.

Though our simulations do not cover enough time of cluster mass loss, it might be interesting to look for signs of velocity anisotropies in our runs. Following Binney & Tremaine (1986), we define an anisotropy parameter β as,

$$\beta = 1 - \frac{v_t^2}{2v_r^2},$$

where v_r and v_t are the radial and tangential velocity dispersions respectively. They are measured in a non-rotating coordinate system in which the cluster centre is always at rest at the origin.

Fig. 14 shows the radial variation of β for models m9 and m3 at various times. All models show radial anisotropy in the outer parts of the clusters. The velocity anisotropy is expected to be changed with time. We can see that the radial anisotropy decreases with time. Extra-tidal stars also show radial anisotropy and do not show clear difference from outermost parts of bounded stars. From Fig. 14, we also confirm the development of radial anisotropy in the outer parts, and that the radial anisotropy decreases with time. Except for the outermost parts, clusters are nearly isotropic and there is no sign of the radially anisotropic velocity dispersion which forms in isolated clusters. Mass segregation could be a reason. Since massive stars are more centrally concentrated, they tend to be located at lower energy levels which have more isotropic velocity distributions (Baumgardt & Makino 2003).

4 SUMMARY AND CONCLUSIONS

We have carried out a dozen N-body simulations of the globular clusters within the external tidal field. Our main conclusion can be summarized as follows:

- (i) All runs show very quick development of tidal tails within a few orbits.
- (ii) Mass segregation effect appears in all runs while the initial mass function is still being preserved. Since the rate of stellar evaporation depends on the mass of the stars, the mass function would change substantially when the amount of evaporated stars becomes more than 50% of the initial mass.
- (iii) The radial distribution of extra-tidal stars can be described by a power law with a slope around -3.2 . This result is well consistent with previous study (Combes et al. 1999). In addition, the radial profile of massive stars have shallower slope in the outer part of the cluster than that of less massive stars as observed in M92 (Lee et al. 2003). This could be a part of the reason why the observational data have shallower slopes than predicted by simulations.
- (iv) The directions of tidal tails are determined by the location of the cluster and its orbits. The length of tidal tails increases towards the apocentre and then decreases towards pericentre. When the length of tidal tails decreases some of the stars in the tails are recaptured by the host cluster. In addition, we verified that the external potential plays an important role in destruction of a cluster.
- (v) The clusters which have no initial angular momentum gain angular momentum from tidal interactions with galaxy. Angular momentum of model clusters gradually increases with time. The model clusters having elongated orbits show rapid increases in angular momentum just after the perigalactic passages.
- (vi) The rotating clusters accelerated by tidal torque start with the rotational angular speed decreasing towards the centre but evolve towards the rigid-body rotation.

(vii) In the early stages of globular cluster evolution, the clusters have radial anisotropy in the outermost parts, while clusters are nearly isotropic in the central region. And the radial anisotropy decreases with time.

These N-body simulations help to understand the recent observations of extended tidal tails around globular clusters. In this study we did not consider tidal shock by galactic disk for simplicity. However disk shock also plays important role in the evolution of globular clusters (Gnedin et al. 1999). Disk component should be contained in subsequent studies to reproduce more realistic Galaxy models. Although we used many particles to reproduce real clusters as possible, it is still far from the real ones. It is necessary to perform N-body simulations with large number of stars up to $N \sim 10^5$.

ACKNOWLEDGMENTS

This work was supported by KRF grant No. 2002-041-C00123. Numerical calculation was carried out by supercomputers at KISTI through Grand Challenge Program. H.S. acknowledges the support of the Korea Science and Engineering Foundation (KOSEF) to the Astrophysical Research Center for the Structure and Evolution of the Cosmos (ARCSEC) at Sejong University.

REFERENCES

- Aarseth S. J., 1999, *PASP*, 111, 1333
- Aarseth S. J., 2004, *Gravitational N-Body Simulations*. Cambridge Univ. Press
- Ahmad A., Cohen L., 1973, *J. Comput. Phys.*, 12, 389
- Baumgardt H., Makino J., 2003, *MNRAS*, 340, 227
- Binney J., Tremaine S., 1987, *Galactic Dynamics*. Princeton Univ. Press
- Combes F., Leon S., Meylan G., 1999, *A&A*, 352, 149
- Davoust E., Prugniel P., 1990, *A&A*, 230, 67
- Einsel C., Spurzem R., 1999, *MNRAS*, 302, 81
- Frenk C. S., Fall M., 1982, *MNRAS*, 199, 565
- Giersz M., Heggie D. C., 1993, in Smith G. H., Brodie J. P. eds, *ASP Conf. Ser. Vol. 48, The Globular Cluster - Galaxy Connection*. Astron. Soc. Pac., San Francisco, p. 713
- Giersz M., Heggie D. C., 1997, *MNRAS*, 286, 709
- Gnedin O. Y., Lee H. M., Ostriker J. P., 1999, *ApJ*, 522, 935
- Grillmair C. J., Freeman K. G., Irwin M., Quinn P. J., 1995, *AJ*, 109, 2553
- Henon M., 1961, *Ann. d'Ap.*, 24, 369
- Keenan D. W., 1981, *A&A*, 95, 340
- Kim E., Einsel C., Lee H. M., Spurzem R., Lee M. G., 2002, *MNRAS*, 334, 310
- Kim E., Lee H. M., Spurzem R., 2004, *MNRAS*, 351, 220
- King I. R., 1966, *AJ*, 71, 64
- Lee C. W., Lee H. M., Ann H. B., Kwon K. H., 1999, *ApJ*, 513, 242
- Lee H. M., Goodman J., 1995, *ApJ*, 443, 109
- Lee H. M., Ostriker J. P., 1986, *ApJ*, 310, 176
- Lee H. M., Fahlman G. G., & Richer H. B., 1991, *ApJ*, 366, 455

- Lee K. H., Lee H. M., Fahlman G. G., Lee M. G., 2003, AJ, 126, 815
- Lee K. H., Lee H. M., Fahlman G. G., Sung H., 2004, AJ, 128, 2838
- Leon S., Meylan G., Combes F., 2000, A&A, 359, 907
- Makino J., 1991, ApJ, 369, 200
- Merritt D., Meylan G., Meyor M., 1997, AJ, 114, 1074
- Meylan G., Heggie D. C., 1997, A&AR, 8, 1
- Meylan G., Meyor M., 1986, A&A, 166, 122
- Odenkirchen M. et al., 2001, ApJ, 548, L165
- Odenkirchen M. et al., 2003, AJ, 126, 2385
- Spitzer L., 1987, Dynamical Evolution of Globular Clusters. Princeton Univ. Press
- Spitzer L., Hart M. H., 1971, ApJ, 164, 399
- Spurzem R., 1999, The Journal of Computational and Applied Mathematics (JCAM), 109, 407
- Spurzem R., Baumgardt H., 2002, MNRAS, submitted
- Takahashi K., Lee H. M., 2000, MNRAS, 316, 671
- Testa V., Zaggia S. R., Andreon G. L., Scaramella R., Djorgovski S. G., de Carvalho R., 2000, A&A, 356, 127
- White R. E., Shawl S. J., 1987, ApJ, 317, 246
- Yim, K. J., Lee, H. M., 2002, J. of Korean Aston. Soc., 35, 75